# On the Inefficiency of Moist Geostrophic Turbulence: A Theory for the Energetic Output under Subsaturated Conditions

MARGUERITE BROWND, a,b OLIVIER PAULUIS, AND EDWIN P. GERBERC

<sup>a</sup> Université du Québec à Montréal, Montréal, Quebec, Canada <sup>b</sup> University of Toronto, Toronto, Ontario, Canada

<sup>c</sup> Center for Atmosphere Ocean Science, Courant Institute of Mathematical Sciences, New York University, New York, New York

(Manuscript received 20 September 2024, in final form 4 September 2025, accepted 17 September 2025)

ABSTRACT: The equator-to-pole temperature gradient has traditionally been understood as the primary driver of the midlatitude storm tracks, which derive their kinetic energy in the process of transporting sensible heat down the gradient. Latent heat, however, accounts for an estimated 30%–60% of the meridional energy transport, a portion which is likely to increase in a warmer world. The contribution of latent heat to the energetics is complicated in that it is inefficient: Only a fraction of the transported latent heat is converted into kinetic energy. Currently, there is no complete theory to explain the relationship between meridional energy transport and kinetic energy generation by midlatitudes eddies. We use a two-layer moist quasigeostrophic model to develop a theory of how the energetic output of the midlatitude atmosphere depends on the relative humidity structure. By varying the surface evaporation rate, we show that the system only reaches the maximum possible energetic output in the saturated limit, producing substantially less kinetic energy at lower evaporation rates. We quantify this reduction in kinetic energy production in terms of a moist conversion efficiency. Using a moist energetic framework, we identify that precipitation dissipation and the diffusion of moisture in subsaturated regions account for the reduction in energetic output. We then show that the moist conversion efficiency can be diagnosed from the distribution of humidity.

SIGNIFICANCE STATEMENT: The impact of humidity on the strength of midlatitude storms is not well understood. Humidity will increase as the planet warms, but it is unclear whether storms will become stronger or weaker as a result. We use an idealized computer model to learn how humidity will impact the strength of storms. We focus on the effect of evaporation at the planet's surface, with simulations ranging from a completely dry atmosphere to one with rain everywhere. In between these two limits, it is raining in only part of the atmosphere, and storms are much weaker than in the case with rain everywhere. We discuss how to connect these results to more complex models and real-world data.

KEYWORDS: Energy transport; Turbulence; Storm tracks; Moisture/moisture budget; Quasigeostrophic models

### 1. Introduction

Predicting the intensity of the midlatitude storm tracks is an ongoing challenge in climate forecasting. CMIP simulations of warming scenarios in recent decades have underestimated both the intensification of the Southern Hemisphere storm tracks and the transport of moist static energy across them (Chemke et al. 2022). Storm activity increases despite relatively little change in the zonally averaged equator-to-pole temperature gradient and baroclinicity, which are traditionally understood as the primary drivers of storms in the midlatitudes. More recently, Kang et al. (2024) demonstrated that prescribing the sea surface temperature in AMIP6 models resulted in Southern Hemisphere storm activity and moist static energy transport that increased within error of the reanalysis trends. However, reanalysis trends exhibit significant uncertainty, demonstrating the need for a better understanding of what processes contribute to increased storminess.

Brown's current affiliation: UQAM, Montreal, Quebec and UofT, Toronto, Ontario, Canada.

Corresponding author: Marguerite Brown, brown.marguerite\_lynette@uqam.ca

Models project the relative humidity of the atmosphere to remain constant with warming (Soden and Held 2006; Sherwood et al. 2010; Merlis et al. 2024), implying that the equator-to-pole humidity gradient increases by  $\sim 7\%$  K<sup>-1</sup> for a uniform warming. Even if the temperature gradient decreases, the humidity gradient is expected to increase due to the exponential increase in saturation vapor pressure with temperature: The absolute water vapor content of the low latitudes will increase more rapidly than that of the high latitudes. Because humidity and temperature interact when latent heat is released through condensation, moist processes contribute to a tug of war on the eddy kinetic energy (EKE) of the storm tracks (Shaw et al. 2016), with some factors contributing to increases and others to decreases. These opposing influences mean that the impact of moisture on the size, frequency, and propagation of storms can change, even if latent heat is not the primary driver of changes to the total energetics (e.g., Lorenz and DeWeaver 2007; O'Gorman 2010). An updated theory for the energetics of the midlatitude storm tracks which includes the impact of moisture is necessary to understand their response to global warming and other forcings.

This study develops a theoretical framework for how moisture impacts the kinetic energy of the midlatitude atmosphere, with an emphasis on how the subsaturation of the atmosphere, that is, the fact that the relative humidity of the atmosphere is generally far from 100%, limits mechanical output. We use an

DOI: 10.1175/JAS-D-24-0179.1

<sup>© 2025</sup> American Meteorological Society. This published article is licensed under the terms of the default AMS reuse license. For information regarding reuse of this content and general copyright information, consult the AMS Copyright Policy (<a href="https://www.ametsoc.org/PUBSReuseLicenses">www.ametsoc.org/PUBSReuseLicenses</a>).

idealized framework, the moist quasigeostrophic (MQG) model of Lapeyre and Held (2004), which is particularly well suited for our purpose as it features a uniform background evaporation that tunes the relative humidity.

In our first paper, Brown et al. (2023) discussed the energetics of MQG under very high evaporation, which keeps the atmosphere at saturation nearly everywhere. Our analysis introduced the concept of moist energy (ME), a quadratic term quantifying moisture fluctuations. In the saturated limit, downgradient moisture transport acts as a source for the eddy moist energy (EME), which is converted into EKE, with more intense eddies, a stronger inverse cascade, and a larger eddy-containing scale than in a dry atmosphere with the same meridional temperature gradient.

However, precipitation only occurs over a small fraction of the atmosphere, and this saturated limit is far from our current climate. It therefore does not accurately capture the impact of moisture on the energetics of Earth's storm tracks. The original experiments of Lapeyre and Held (2004) use a lower evaporation rate and, consequently, feature large unsaturated regions. Even though the background moisture gradient is the same, the kinetic energy is reduced relative to our near-saturated integrations with stronger evaporation. We argue that the energetics of moist geostrophic turbulence depend not only on the moisture and temperature gradients but also on the portion of the domain that is unsaturated. We consider a wider range of evaporation rates to explore the transition from low to high relative humidity and address the question: How does the injection of energy through evaporation (latent heat) at the surface impact the production of kinetic energy? In particular, how does this transition vary with the strength of background gradients in temperature and moisture? We define and develop a moist conversion efficiency as a measure of how moisture fluxes are converted into EKE, as compared with the saturated case, which we take to be full efficiency. We show that the moist conversion efficiency increases rapidly at low evaporation and then gradually converges to a saturated limit at high evaporation. We further explore how moist systems lose EME through small-scale diffusion and dissipation due to moist processes.

Section 2 provides context for this study, reviewing past work on the impact of moisture on midlatitude atmospheric dynamics. Section 3 briefly introduces the MQG system and the underlying energetic framework, with an emphasis on the generation and dissipation of EME. Section 4 investigates how mechanical efficiency manifests itself in MQG. Section 5 defines a "moisture conversion efficiency" and the mechanisms that regulate it. Section 6 synthesizes the results of the previous section and introduces a parameter that predicts the moisture conversion efficiency. Section 7 concludes the study.

## 2. Background

In this work, we focus on how moisture impacts energetics using intuition from "dry" geostrophic theory. The atmosphere acts as a heat engine, generating kinetic energy through the downgradient transport of heat. In the tropics, this manifests as energy transport from the warm surface to the cold top of the atmosphere. The midlatitudes additionally feature a significant meridional temperature gradient, resulting in a redistribution

of heat from the tropics to the poles. The result is a baroclinic system with synoptic-scale storms, the intensity of which is constrained by the efficiency of the midlatitude heat engine (e.g., Barry et al. 2002).

To translate this intuition to a moist framework, we need two key adjustments. First, the heat transport must include latent heat. In the current climate, latent heat accounts for between one-third and one-half of the poleward energy transport in the midlatitudes (Lorenz 1978), a portion expected to increase in a warmer world (Frierson et al. 2006). Second, the introduction of moisture fundamentally affects the efficiency of heat engines. Pauluis (2011) shows that the mechanical output of the thermodynamic cycle involving moist air is greatly constrained by the degree of saturation in the cycle. A saturated cycle—one where the system is everywhere at the saturation value set by the Clausius-Clapeyron relation—generates the same mechanical output as a Carnot cycle. A partially saturated cycle is significantly less efficient. Evaporation of liquid water in unsaturated air, diffusion of water vapor, and falling rainfall are irreversible processes that can greatly reduce the mechanical output of a moist atmosphere. This effect has been demonstrated for convection (Pauluis and Held 2002a,b; Singh and O'Gorman 2016), tropical cyclones (Pauluis and Zhang 2017), and the general global circulation (Laliberté et al. 2015). A theory for moist geostrophic turbulence must address these two aspects: the enhancement of the meridional heat transport by the inclusion of latent heat and the reduction of mechanical output due to irreversible moist processes.

Indeed, moisture has been observed to have competing effects on processes relevant to the midlatitude storm tracks. Moisture can intensify instabilities by reducing the effective stratification for ascending parcels (Emanuel et al. 1987; Lapeyre and Held 2004; Lambaerts et al. 2011; Schneider and O'Gorman 2008). The theory behind these localized instabilities has primarily been developed in linearized systems with highly parameterized moisture that is assumed to be continuously available without an explicit evaporation term. These studies have provided useful insights into the scale, growth, and evolution of such instabilities (Whitaker and Davis 1994; Parker and Thorpe 1995; Moore and Montgomery 2004; Adames and Ming 2018; Kohl and O'Gorman 2022) that are borne out well in mesoscale models (Moore and Montgomery 2005), GCMs (O'Gorman et al. 2018), and reanalysis data (Wernli et al. 2002; Moore et al. 2008). However, they provide limited insight into how the availability of moisture, governed by planetary constraints such as the evaporation rate and poleward transport of latent heat, determines the frequency of such instabilities.

For equilibrated systems (e.g., radiative–convective equilibrium, quasi equilibrium), moisture weakens the flow. In the midlatitudes, the poleward transport of latent heat reduces EKE by changing the temperature structure of the atmosphere. This effect is especially pronounced in the presence of a nonhomogeneous background gradient, e.g., a Bickley jet, where precipitation poleward of the jet flattens the meridional temperature gradient (Bembenek et al. 2020; Lutsko and Hell 2021). Furthermore, when changes to the dry static stability at least partially compensate for the destabilizing effect of a moister atmosphere (Juckes 2000; Zurita-Gotor 2005; Frierson 2006), moist baroclinic growth

occurs less frequently, restricting the growth of EKE on average over long time periods.

We propose that the combined effect of moisture on the midlatitude storm tracks hinges on how efficiently moisture fluxes are converted into EKE as a function of mean moisture deficit, or the degree to which the atmosphere is subsaturated. Indeed, the initial distribution of moisture has been shown to significantly impact the total energetics in eddy life cycles (Pavan et al. 1999). Implicitly underlying this result is the interplay between the generation of small-scale moisture variance by turbulent mixing and its removal by diabatic processes. We show that the portion of the domain at saturation influences the energetics of the system by determining the predominant process by which moisture anomalies are removed. Subsaturated regions tend to mix moisture to smaller scales, resulting in the removal of moisture anomalies by dissipation. The same process can result in highly localized condensation and the formation of isolated vortices. In contrast, highly saturated systems tend to convert moisture anomalies into temperature anomalies at scales larger than the turbulent dissipation scale. Consequently, the degree of saturation determines the mechanical output of moist geostrophic turbulence.

In Brown et al. (2023), we showed how the inclusion of the meridional latent heat transport greatly enhances geostrophic turbulence in the saturated limit. Using MQG with high evaporation and fast precipitation adjustment, we found that a greater bulk moisture stratification significantly increases the generation of kinetic energy and elongates the inverse cascade of the barotropic flow. We focused solely on the limiting case of a saturated atmosphere, where precipitation occurs everywhere. The saturated limit has the advantage of being mathematically equivalent to a dry model after a rescaling based on the gross moisture stratification, but circumvents the more difficult issue of how much kinetic energy is generated in a partially saturated atmosphere. Here, we focus on the transition from the dry to saturated limits, where irreversible moist processes play a critical role.

### 3. Model description

As in Brown et al. (2023), we use the MQG model of Lapeyre and Held (2004) (Fig. 1), a two-layer model on a  $\beta$  plane with moisture constrained to the bottom layer. The evolution of the system is described by the equations:

$$\frac{D_1}{Dt}(\zeta_1 + \beta y) = -f_0 \frac{W}{H} - \nu \nabla^8 \zeta_1, \tag{1}$$

$$\frac{D_2}{Dr}(\zeta_2 + \beta y) = +f_0 \frac{W}{H} - r\zeta_2 - \nu \nabla^8 \zeta_2, \tag{2}$$

$$\frac{D_2}{Dt}\eta = -W + \mathcal{L}P - R - \nu \nabla^8 \eta, \tag{3}$$

$$\frac{D_2}{Dt}\eta_c = -\frac{\mathcal{L}P}{\mu_s - 1} + \frac{E - R}{1 + \mathcal{C}} - \nu \nabla^8 \eta_c, \tag{4}$$

$$P = \begin{cases} 0 & \eta \ge \eta_c \\ (1+\mathcal{C})\frac{\eta_c - \eta}{\tau} & \eta < \eta_c \end{cases}$$
 (5)

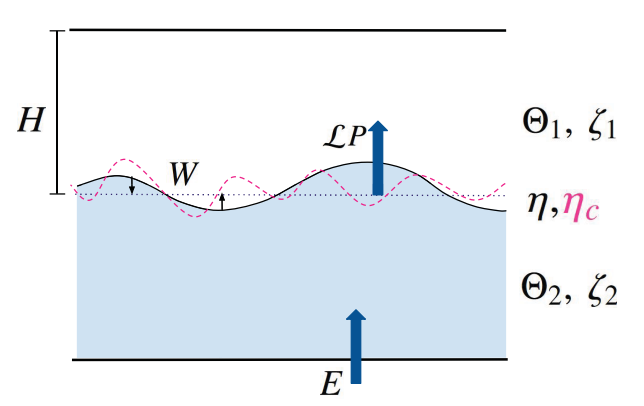


FIG. 1. The MQG model of Lapeyre and Held (2004), consisting of a top- and bottom-layer vorticity  $\zeta_i$ , i=1,2, respectively, an interface thickness  $\eta$ , and a condensation thickness  $\eta_c$ . The moisture is contained to the bottom layer, shaded blue, and precipitation P occurs when the moisture content rises above the condensation thickness, depicted by the dashed magenta line. Vertical motion W adjusts interface anomalies to a reference value. A constant evaporation rate E replenishes the moisture content of the bottom layer, and radiative cooling R raises the interface  $\eta$  and the condensation interface  $\eta_c$ .

We decompose the flow into the top- and bottom-layer vorticity ( $\zeta_1$  and  $\zeta_2$ , respectively). The material derivative of the *i*th layer flow is represented with  $D_i/Dt$ . Each vorticity is advected by the flow in its own layer, while the interface  $\eta$  and condensation interface  $\eta_c$  (a measure of the moisture content, detailed below) are advected by the lower layer. The first term on the right-hand side of the vorticity equations, Eqs. (1) and (2), captures the generation of vorticity by vertical motion (or ageostrophic convergence  $W = H\nabla \cdot \mathbf{u}_1$ ), which can be assessed diagnostically through an  $\omega$  equation (see appendix B of Brown et al. 2023). The second term on the right hand side of Eq. (2) is the Ekman dissipation at the surface. The final term in all prognostic equations is a higher-order numerical dissipation.

Equation (3) captures the evolution of the interface between the two layers, at  $z = H - \eta$ . In quasigeostrophic (QG) theory,  $\eta$  is proportional to the baroclinic streamfunction  $\psi_1 - \psi_2$  via the thermal wind relation  $\eta = H(\psi_1 - \psi_2)/\lambda^2 f_0$ . The Rossby deformation radius  $\lambda = \sqrt{g^* H/f_0}$  is defined in terms of the effective gravity  $g^* = g\delta\theta/\theta_0$ , the reference thickness H, and the reference rotation rate  $f_0$ . Under the assumption that moisture is confined to the lower layer, the interface position  $\eta$  also characterizes the maximum vertical extent of water vapor. The interface is additionally forced by latent heat release in response to precipitation P and dissipated by a constant radiative cooling R. The strength of latent heating relative to the vertical stratification is characterized by the nondimensional parameter  $\mathcal{L} = L_q m_0 / (c_p \delta \theta)$ , where  $L_q$  is the strength of latent heating,  $m_0$  is a reference moisture content, and  $c_p$  is the specific heat capacity at constant pressure.

Following Brown et al. (2023), Eq. (4) governs the condensation thickness  $\eta_c$ , constructed as a moisture equation independent of ageostrophic convergence. The condensation height is defined by

$$\eta_c = \frac{\eta + m}{1 + C} = \eta + \frac{m - C\eta}{1 + C}.$$
 (6)

Here, m is a thickness-equivalent water vapor mixing ratio, defined relative to a reference value  $m_0$  such that the total mixing ratio is given by  $m_0(1 + m/H)$ . Moisture is contained exclusively in the bottom layer, governed by the equation:

$$\frac{D_2}{Dt}m = +W - P + E. (7)$$

The mixing ratio is increased by ageostrophic convergence W in the lower layer, removed by precipitation P, and continuously replenished by evaporation E from the surface. The evaporation is constant and uniform, so that there is a constant relation between radiative cooling and evaporation,  $R = \mathcal{L}E$ .

Precipitation occurs when the moisture content exceeds saturation. We define the saturation value  $m_s$  by a linearization of the Clausius-Clapeyron relation:

$$m_{s} = C\eta,$$
 (8)

where  $\eta$  corresponds to temperature in the QG framework. In the regions where the moisture content exceeds saturation  $(\eta_c > \eta)$ , the system is supersaturated, as illustrated in Fig. 1 where  $\eta$  (the solid black line) rises above the condensation level  $\eta_c$  (the dotted pink line), recalling that a positive value of  $\eta$  implies a downward shift of the interface (see also Fig. 2 of Brown et al. 2023). When supersaturation occurs, precipitation P, determined in Eq. (5), relaxes the condensation level to the interface level with characteristic time  $\tau$ .

Precipitation reduces the effective static stability of the system; the strength of the reduction is determined by the amount of latent heat release. Moisture surpluses (i.e., subsaturated regions) arise from both the meridional and vertical transport of moisture, where in the two-layer model, vertical transport corresponds to the increase in m from the +W term in Eq. (7). The gross moist stratification is therefore defined relative to both the vertical and meridional moisture gradients:

$$\mu_s^{-1} = \frac{1 - \mathcal{L}}{1 + CC},\tag{9}$$

where  $\mathcal{L}$  is proportional to the reference moisture content of the lower layer  $m_0$  and inversely proportional to the layer temperature difference  $\delta\theta$ .

Each prognostic equation contains an eighth-order diffusion term dominant at small scales. As we will show, this term is a significant sink of the condensation thickness. In all other equations, it acts to maintain numerical stability but has an otherwise negligible role in the dynamics.

Both the interface and the condensation level have a homogenous background gradient:

$$\overline{\eta} = \overline{\eta}_c = -U\lambda^{-2}y,\tag{10}$$

where the overbar indicates a zonal average and *U* is a reference wind shear. Equivalently, the background meridional moisture gradient is proportional to the temperature gradient

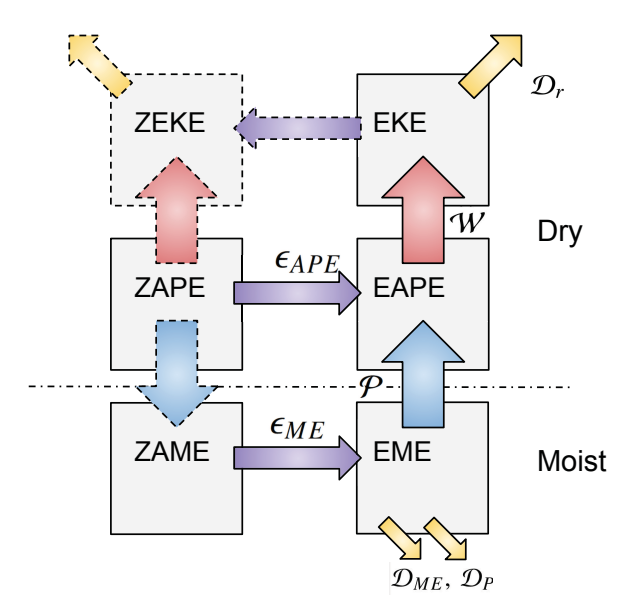


FIG. 2. A modified Lorenz cycle for the MQG system. In the classical dry Lorenz cycle of a homogeneous two-layer QG system, depicted above the dotted–dashed line, EAPE is generated when the downgradient flux of the thickness ( $\varepsilon_{\rm APE}$ ) converts the zonally averaged ZAPE into EAPE, respectively. The EAPE is converted into EKE through vertical motions and lost through Ekman dissipation ( $\mathcal{D}_r$ ). The dashed borders indicate terms that would be included in the full Lorenz cycle but do not impact in our QG model. Moisture modifies this cycle through the injection of precipitation  $\mathcal{P}$  into the APE. However, this transfer accounts for only a portion of the EME generated from the ZAME by the downgradient flux of the condensation thickness ( $\varepsilon_{\rm ME}$ ). The remainder of the EME is lost through small-scale diffusion  $\mathcal{D}_{\rm ME}$  and eddy precipitation dissipation  $\mathcal{D}_P$ . These losses reduce the mechanical efficiency of the full moist system.

by the Clausius–Clapeyron coefficient C. Classic dry baroclinic theory predicts unstable growth when the criticality  $\xi$  exceeds a critical value, i.e.,

$$\xi \equiv \frac{U}{\lambda^2 \beta} > 1. \tag{11}$$

The saturated theory predicts unstable growth based on a saturated criticality:

$$\mu_s \xi \equiv \mu_s \frac{U}{\lambda^2 \beta} > 1. \tag{12}$$

a. Incorporating moist energy into the Lorenz cycle

As in Brown et al. (2023), we split the energy cycle of the MQG system into three parts: 1) kinetic energy, proportional to  $|\mathbf{u}_1|^2 + |\mathbf{u}_2|^2$ ; 2) available potential energy (APE), proportional to  $|\eta|^2$ ; and 3) ME, proportional to  $|\eta_c|^2$ . A modified Lorenz cycle for the energetics of the MQG system, constructed conceptually from exchanges between zonal mean and eddy flow, is depicted schematically in Fig. 2. The classic dry Lorenz cycle is contained above the dotted–dashed line.

A zonally averaged APE is determined by the prescribed meridional gradient of the interface,  $\overline{\eta}_y = -U\lambda^{-2}$ . Downgradient mixing generates eddy APE (EAPE) at rate  $\varepsilon_{\rm APE}$  and converts it into EKE through vertical motion  $\mathcal{W}$ . This EKE is lost at large scales due to Ekman dissipation  $\mathcal{D}_r$ . In a full Lorenz cycle, EKE is converted into a zonally averaged zonalmean kinetic energy (ZKE) which reduces the zonal-mean APE (ZAPE) in the isentropic average by redistributing the large-scale meridional temperature gradient. Because a background state ZKE is prescribed in our homogeneous QG setup, these components are included only for reference via the dashed arrows.

The ME component, below the dashed line, accounts for contributions to latent heat release. We construct the domain-averaged EKE equation by multiplying Eqs. (1) and (2) by their respective streamfunction perturbation, averaging, and taking the sum. Similarly, the domain-averaged dry EAPE equation is obtained by multiplying Eq. (3) by the interface perturbation  $\eta'$  and a constant  $g^*/2H$  and the domain-averaged EME equation by multiplying Eq. (4) by the condensation-level perturbation  $\eta'_c$  and a constant  $g^*(\mu_s-1)/2H$ , and then averaging and summing over the two levels. This yields

$$\partial_r EKE = +W - D_r,$$
 (13)

$$\partial_t \text{EAPE} = +\varepsilon_{\text{APE}} - W + \mathcal{P},$$
 (14)

$$\partial_t \text{EME} = +\varepsilon_{\text{ME}} - \mathcal{P} - \mathcal{D}_{\text{ME}} - \mathcal{D}_P,$$
 (15)

where the script terms are defined in Table 1. The EKE receives injections from vertical motions  $\mathcal{W}$  near the Rossby deformation radius and dissipates energy at the largest scales through the Ekman term  $\mathcal{D}_r$ . The energy injection from vertical motion corresponds to a reduction in the APE. APE is generated from the meridional sensible heat flux  $\varepsilon_{\text{APE}}$  and precipitation injection  $\mathcal{P}$ . The key modification from the dry cycle is in the precipitation term  $\mathcal{P}$ , which converts ME into APE. With the inclusion of precipitation, the APE scales with the total EKE, like the moist APE (MAPE) of, e.g., Lorenz (1978) and O'Gorman and Schneider (2008).

As in Brown et al. (2023), the ME is constructed from a quadratic of the condensation thickness to isolate the precipitation conversion. EME is generated by the condensation thickness flux  $\varepsilon_{\text{ME}}$ . Like the sensible heat flux, this term redistributes the planetary-scale gradient of the condensation thickness. At full saturation, MQG systems fully convert the condensation thickness flux into EAPE through precipitation. We will show that partially saturated systems convert only a fraction of the condensation thickness flux into EAPE.

The two final terms on the right-hand side of Eq. (15) characterize pathways for the loss of EME that do not produce available potential energy:  $\mathcal{D}_{\text{ME}}$  and  $\mathcal{D}_{p}$ . The first quantifies the irreversible, small-scale diffusion of moisture, given by

$$\mathcal{D}_{\text{ME}} = \frac{g^*(\mu_s - 1)}{2H} \nu \langle |\nabla^4 \eta_c'|^2 \rangle, \tag{16}$$

where the angle brackets indicate a time and domain average. In equilibrated dry systems, where moisture is a passive tracer,

TABLE 1. Generation, transfer, and dissipation terms for the kinetic energy and MAPE.

minette energy and ivit if 2.				
EKE	$\langle u_1'^2 + u_2'^2 \rangle / 2$	Eddy kinetic energy		
EAPE	$g^*\langle  \eta' ^2 \rangle/2H$	Eddy available potential energy		
EME	$g^*(\mu_s - 1)\langle  \eta_c' ^2 \rangle / 2H$	Eddy moist energy		
$\mathcal{D}_r$	$r\langle  u_2' ^2\rangle$	Ekman dissipation		
W	$f_0 \langle W' \eta'  angle / H$	APE to EKE injection (vertical motion)		
$arepsilon_{ ext{APE}}$	$-g^*\overline{\eta}_{_{_{\boldsymbol{\mathcal{V}}}}}\langle \upsilon_2'\eta'\rangle/2H$	Sensible heat flux		
$arepsilon_{ m ME}$	$-g^*(\mu_s-1)\overline{\eta}_v\langle \nu_2'\eta_c'\rangle/2H$	Condensation thickness flux		
$\mathcal{P}$	$g^*\mathscr{L}\langle P'\eta' angle/2H$	ME to APE injection (precipitation)		
$\mathcal{D}_{ ext{ME}}$	$g^*(\mu_s - 1)\nu\langle \nabla^4\eta_c' ^2\rangle/2H$	High-order diffusion		
$\mathcal{D}_P$	$g^* \mathscr{L} \langle P'(\eta'_c - \eta') \rangle / 2H$	Precipitation dissipation		

this is the only means of removing EME. As an eighth-order diffusion term, this term dominates at small scales. Small-scale diffusion is therefore largest in flows where a strong forward cascade results in substantial convergence of moisture to scales smaller than the deformation radius. In the saturated case, this term is negligible because precipitation terminates the forward cascade at scales larger than the diffusion scale (Brown et al. 2023).

The second pathway for the loss of EME in partially saturated systems is eddy precipitation dissipation:

$$\mathcal{D}_{P} = \frac{g^{*}}{2H} \langle \mathcal{L}P'(\eta'_{c} - \eta') \rangle. \tag{17}$$

The nonlinearity of the precipitation term complicates the impact of this dissipation on the EME, as precipitation only occurs in the regions where the eddy surplus exceeds the domain-mean deficit denoted by the subscript 0, i.e.,

$$\eta_c' - \eta' > \eta_0 - \eta_{c,0}.$$
 (18)

The eddy surplus is thus constrained by

$$\eta'_c - \eta' \le \frac{\tau P}{1 + C} - \eta_{c,0} + \eta_0.$$
 (19)

Because equality occurs in precipitating regions, we multiply both sides by the precipitation P and take the domain average to obtain

$$\langle P'(\eta'_c - \eta') \rangle = \frac{\tau \langle P'^2 \rangle}{1 + C} + \frac{\tau P_0^2}{1 + C} - P_0(\eta_{c,0} - \eta_0).$$
 (20)

To determine the sign of this term, let us consider the perturbation and domain-average terms separately. The first term on the right-hand side is a quadratic of the precipitation anomaly and only removes EME. The domain average of Eq. (19) implies that the remaining terms are, in combination, greater than zero, making  $\mathcal{D}_P$  a sink of EME.

In both the dry and saturated limits,  $\mathcal{D}_p$  vanishes. In the dry limit, there is no precipitation and, therefore, no precipitation

TABLE 2. Tunable parameter space (nondimensionalized), realistic values, and the values used in the simulations. Here, $E^*$ is the					
dimensional evaporation parameter, and $E$ is the nondimensionalized parameter.					

Parameter	Expression	Realistic	Represents	Simulation values
ξ	U	1	Dry criticality	0.8, 1.0, 1.25
$\mu_s$	$\frac{\overline{\beta\lambda^2}}{1 + \mathcal{CL}}$	≈1.75–2.62	Gross moist stability	1.75, 2.62, 4
E	$rac{1-\mathcal{L}}{rac{f_0\lambda^2}{U^2m_0}E^*}$	0.4	Evaporation rate	$(0, 1, 2, 5) \times (10^{-1}, 10^{0}, 10^{1}, 10^{2})$
$\mathcal{R}$	$r\lambda$	0.16	Ekman damping	0.16
$ au^*$	$rac{\overline{U}}{\lambda}$	<0.15-0.85	Precipitation time scale	0.001 25
$L/\lambda$	$\stackrel{\lambda}{L/\lambda}$	_	Domain size	$18\pi$
dt	$\Delta t U$	_	Time step	0.00025
$ u^*$	$\stackrel{\lambda}{U\lambda^7} u$	_	Small-scale dissipation	$10^{-7}$

dissipation. In the saturated limit, moisture and temperature are perfectly correlated, so  $\eta_c' - \eta' = 0$ . In partially saturated systems, moisture and temperature anomalies are not correlated, so precipitation dissipation removes EME and reduces the total conversion to EAPE. This selectively flattens positive moisture anomalies, resulting in an asymmetric reduction in moisture variance and a shift to a larger average moisture deficit.

### b. Dry and saturated limits

The above dynamical system has two limiting cases. In the dry limit, moisture acts as a passive tracer, mixed by turbulent dynamics to the diffusion scale. In the saturated limit, strong evaporation and fast precipitation adjustment times results in a system that is raining everywhere and rapidly adjusts the moisture profile to the saturation value set by the Clausius-Clapeyron relation. The dry limit is achieved under the condition E = 0.0 after sufficient simulation time for the initial distribution of water vapor to reach a statistically equilibrium state. Brown et al. (2023) showed that the saturated limit is achieved in this system in the limit of high evaporation  $(E = 1000U^2m_0/f_0\lambda^2)$  and fast precipitation relaxation time ( $\tau = 0.00125 \lambda/U$ ). This saturated limit behaved as the dry limit with shorter length and faster time scales, characterized by powers of  $\mu_s$ . Hence, the saturated system exhibits significantly faster eddy growth, smaller-scale instabilities, and overall higher EKE compared with the dry case. In both limits, downgradient heat fluxes are converted into EKE with near perfect efficiency.

Partially saturated systems exhibit reduced mechanical efficiency compared with both saturated and dry systems. The dissipation terms described in the previous section, which were negligible in the saturated case, become quite significant in the partially saturated case. We explore the transition from the dry limit to the saturated limit by considering systems with intermediate evaporation rates, so that precipitation occurs but only locally. This localization creates a nonlinearity such that moisture is neither a fully passive tracer (as in the dry case) nor correlated with temperature (as in the saturated case). We expect the partially saturated case to act as a combination of the dry and saturated cases.

### c. Numerical experiments

Our experiments bridge the gap between the moisture gradient sweeps in the partially saturated (Lapeyre and Held 2004) and saturated (Brown et al. 2023) cases. We fix the moisture and temperature gradients while varying the evaporation rate *E* to adjust the degree of saturation, i.e., the portion of the domain that is precipitating. Increasing the evaporation rate also increases the domain-averaged relative humidity of the system.

Experiments are done on the same system as in Brown et al. (2023). A complete list of the nondimensional parameters used is in Table 2. The domain size is  $L = 18\pi\lambda$ , with time steps of size  $dt = 0.00025 \lambda/U$ . Small-scale dissipation  $\nu =$  $10^{-7} \lambda^7 U$  is chosen to avoid damping small-scale energy generation associated with moist effects on the scales of instability. The precipitation time scale  $\tau = 5dt$  is chosen to enforce rapid adjustment, and Ekman damping  $r = 0.16U\lambda^{-1}$  is in line with the value used by Held and Larichev (1996). The values of the dry criticality  $\xi$  are chosen to be near the Earth-like value of 1. The values of  $\mu_s$  are informed by the range of realistic seasonand hemisphere-averaged values. We used simulations with C = 2.0 and L = .2, .35, .5, corresponding to  $\mu_s = 1.75, 2.62$ , 4.0. This roughly corresponds with a Northern Hemisphere winter, Northern Hemisphere summer, and a higher moisture gradient. An additional run with C = 0.0 and L = 0.75 with  $\mu_s = 4.0$  was performed to confirm that simulations with the same value of  $\mu_s$  behave similarly for the metrics we use.

We chose the range of the moisture gradient based on a number of factors. First, on local scales, such as in the warm sector of surface cyclones (e.g., Emanuel 1985), latent heat release can fully overcome the dry static stability of the atmosphere, i.e.,  $\mathcal{L} \to 1$ ,  $\mu_s \to \infty$ . Second, the moisture stratification and meridional gradients are expected to increase in warmer climates. Third, idealized models corresponding to  $\mu_s > 3.33$  have exhibited a transition to a vortex-dominated regime (e.g., Kohl and O'Gorman 2022), so higher moisture stratification may indicate a different regime of instability. The evaporation is widely varied for the purposes of a parameter sweep, ranging from an essentially dry case (E = 0.0) to a value that is nearly saturated in all of our experiments (E = 100.0).

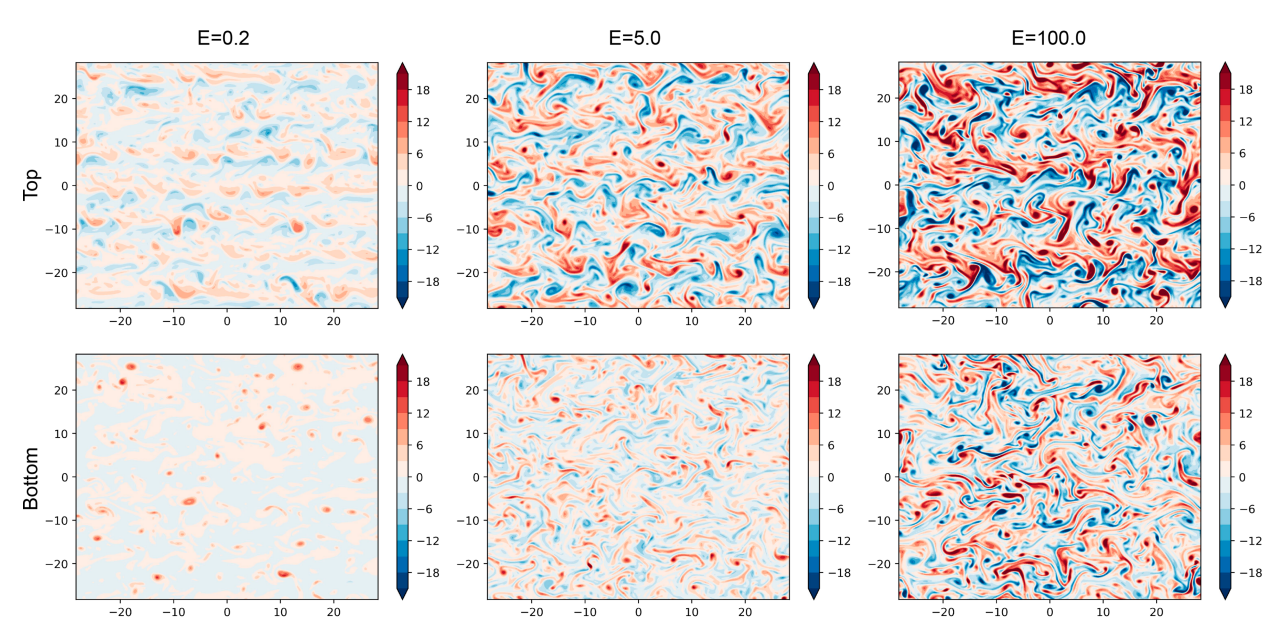


FIG. 3. Snapshots of the top- and bottom-layer relative vorticity for  $\xi = 0.8$ ,  $\mu_s = 4.0$ , with varying evaporation (labeled in each column).

Varying the evaporation rate requires a comparable adjustment of the radiative cooling rate to maintain energy balance at large scales.

# 4. On the efficiency of conversion of ME to KE by precipitation

In midlatitude systems, both sensible and latent heat are mixed downgradient by eddy fluxes. This results in a distribution of both across a wide range of scales. A key feature distinguishing the impact of latent heat from sensible heat is that not all of the water vapor that is moved poleward by the atmosphere is condensed at higher latitudes, and therefore only a portion of the latent heat transport ultimately generates EKE.

In MQG, varying the evaporation rate modifies the amount and distance over which water vapor is displaced before being converted into sensible heat. Figure 3 shows the impact in simulations with  $\xi=0.8$ ,  $\mu_s=4.0$ . At low evaporation (E=0.2), the upper-level flow is organized into seven narrow jets, while the low-level flow exhibits a few intense cyclonic vortices amid a backdrop of weak PV anomalies. At high evaporation (E=5.0), the upper-level flow organizes itself into five jets, and the low-level flow begins to exhibit nearer symmetry in the distribution of cyclonic and anticyclonic extremes. The saturated limit is approached in the limit of extreme evaporation (E=100.0). The upper-level flow organizes into three jets, and the low-level flow features a number of extreme cyclone and anticyclone anomalies.

Figure 4 shows the time- and domain-averaged EKE as a function of the evaporation rate for several parameter sweep experiments with varying dry and moist criticality. In general, the EKE increases with the evaporation rate. Near E=10, EKE converges to a maximum value for the experiments where  $\xi=1.25$ ,  $\mu_s=1.75$ , and  $\xi=0.8$ ,  $\mu_s=1.75$ , 2.62, corresponding to the transition to the saturated limit. We expect

that a similar convergence would occur for all moisture and temperature gradients at sufficiently high evaporation. This reflects the fact that a more turbulent atmosphere acts as a more efficient atmospheric dehumidifier. Consequently, systems with a higher saturated criticality  $\mu_s \xi$  require a higher evaporation rate to achieve saturation. The saturation value of E depends more strongly on the gross moisture stratification  $\mu_s$  than on the dry temperature gradients, characterized by  $\xi$ .

In each set of evaporation sweeps, EKE increases significantly from the dry limit to the E=100 experiment. In the systems with the highest gross moisture stratification, the saturated systems have  $\sim 100$  times the EKE of the corresponding dry simulation. The sweep with  $\xi=1.25$ ,  $\mu_s=1.75$  exhibits the smallest increase in EKE from dry to saturated, with only

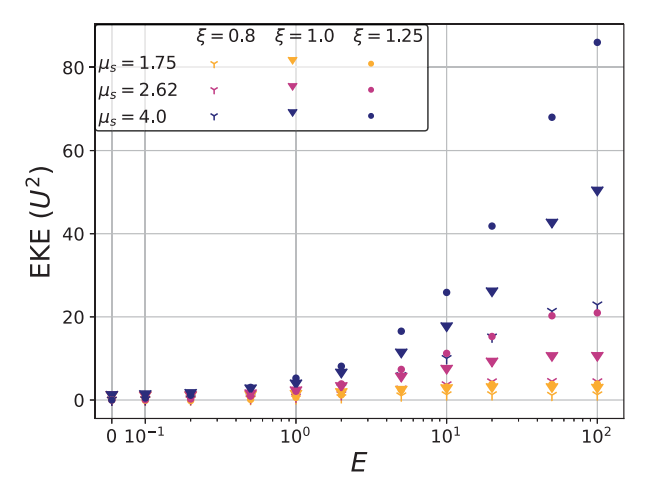


FIG. 4. The total EKE of the system as a function of evaporation for varying combinations of the dry criticality  $\xi$  and gross moist stratification  $\mu_{\kappa}$ .

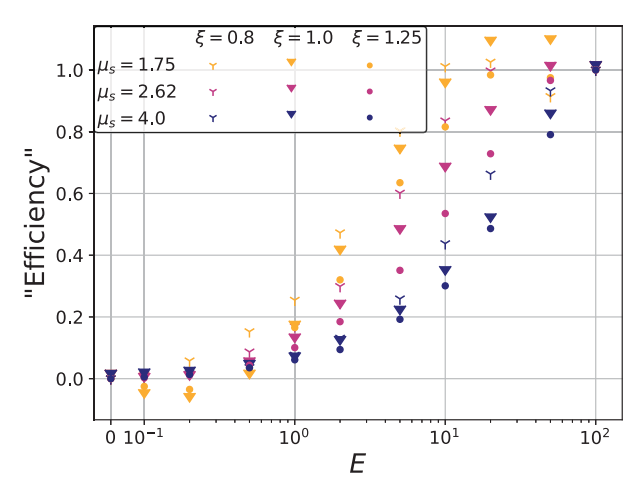


FIG. 5. An empirical estimate of the mechanical efficiency as a function of evaporation.

a factor of  $\sim$ 3 increase. We use the saturated limit studied in Brown et al. (2023) to quantify the EKE of a perfectly efficient moist system. Then, the mechanical output of a partially saturated system relative to the saturated limit can be used to characterize how efficiently it can convert ME into EKE. As a crude metric to capture the "moist efficiency," we compare the EKE of a given system with the value in the dry and saturated limits, i.e.,

"Efficiency" = 
$$\frac{EKE - EKE_0}{EKE_{100} - EKE_0}.$$
 (21)

Here,  $EKE_0$  is the EKE at E=0 and  $EKE_{100}$  is the EKE at E=100, holding the temperature and moisture stratification constant.

Figure 5 shows the distribution of our efficiency metric as a function of evaporation. By definition, this metric enforces zero efficiency in the dry limit (where there is no net latent heat transport) and perfect efficiency for E = 100, although not all configurations have fully reached the saturated limit with E = 100. The spread between the curves in Fig. 5 shows that evaporation alone is not sufficient to predict the efficiency of a moist system. The amount of evaporation needed to achieve near-perfect efficiency increases with both the temperature and moisture gradients. Furthermore, a few of the systems with low moisture stratification ( $\mu_s = 1.75, \xi = 1.0$ , 1.25) exhibit a negative "efficiency" at low evaporation; here, a small amount of evaporation actually reduces the EKE output relative to the dry limit. These results emphasize that impact of changes to the surface latent heat flux depends on the temperature ( $\xi$ ) and moisture ( $\mu_s$ ) structure.

# 5. Generation, loss, and conversion of moist available potential energy

We now more rigorously characterize the moist conversion efficiency of a geostrophic system, seeking to explain how E,  $\mu_s$ , and  $\xi$  cause the efficiency to vary. Per the energetic framework of section 3a, we identify three processes governing the

impact of latent heat on EKE in the MQG system: 1) the conversion from EME to EAPE through precipitation, 2) the generation of ME through the meridional flux of sensible and latent heat, and 3) the loss of EME through diffusion and precipitation dissipation. We quantify the first process by the conversion ratio of the diabatic forcing to the sensible heat flux:

$$r_{\rm con} = \frac{\langle \mathcal{P} \rangle}{\langle \varepsilon_{\rm APE} \rangle}.$$
 (22)

Parker and Thorpe (1995) and Moore and Montgomery (2005) argued that baroclinic growth dominates in systems where this ratio is much less than one, while diabatic effects dominate when the ratio is greater than one. In MQG, the conversion ratio goes to zero in the dry limit:

$$\lim_{E \to 0} r_{\rm con} = 0.$$

In the saturated limit, Brown et al. (2023) showed that this ratio converges to

$$\lim_{E \to \infty} r_{\text{con}} = \mu_s - 1. \tag{23}$$

As a starting point in our discussion of the energetics, we explore how the conversion ratio changes with surface evaporation rate.

Figure 6a plots the conversion ratio as a function of evaporation. In the saturated limit, this ratio converges as predicted to  $\mu_s - 1 \approx 1.62$  and 0.75 for  $\mu_s = 2.62$  and 1.75, respectively, but does not reach the predicted value of 3.0 for  $\mu_s = 4.0$ , consistent with these systems remaining only partially saturated even for very high evaporation rate. Increasing evaporation generally increases the portion of APE generated by precipitation. This transition is sharpest in the case with subcritical baroclinicity and high moisture gradient ( $\xi = 0.8$ ,  $\mu_s = 4.0$ ) between E = 0and E = 0.1, where only a small evaporation rate results in precipitation accounting for ~60% of the APE generation. In comparison, the same evaporation rate and moisture stratification in the  $\xi = 1.25$  case result in a system with precipitation accounting for  $\sim 30\%$  of the APE generation. The  $\xi = 1.0$  case has an evaporation dependency more similar to the  $\xi = 1.25$  case for small E, indicating that the presence of even a small amount of moisture has a much more significant effect under conditions that would be stable in a dry simulation.

This large increase in conversion ratio in the low baroclinicity, high moisture ( $\xi = 0.8$ ,  $\mu_s = 4.0$ ) experiment is reminiscent of the results of Kohl and O'Gorman (2022), where Diabatic Rossby Vortices were found to exhibit the greatest unstable growth in the presence of weakened potential vorticity gradients with a sufficient reduction in static stability. An equivalent configuration in MQG would predict the strongest Diabatic Rossby Vortices for  $\mu_s > 3.33$ ,  $\xi < 1.0$ . It is possible that such a mechanism contributes to the sharp increase in conversion ratio at low evaporation rates. Indeed, the low-level vorticity, shown in Fig. 3, exhibits isolated vortices that are qualitatively consistent with this interpretation.

The generation of both APE and ME relates to the downgradient transport of sensible and latent heat. In a dry system,

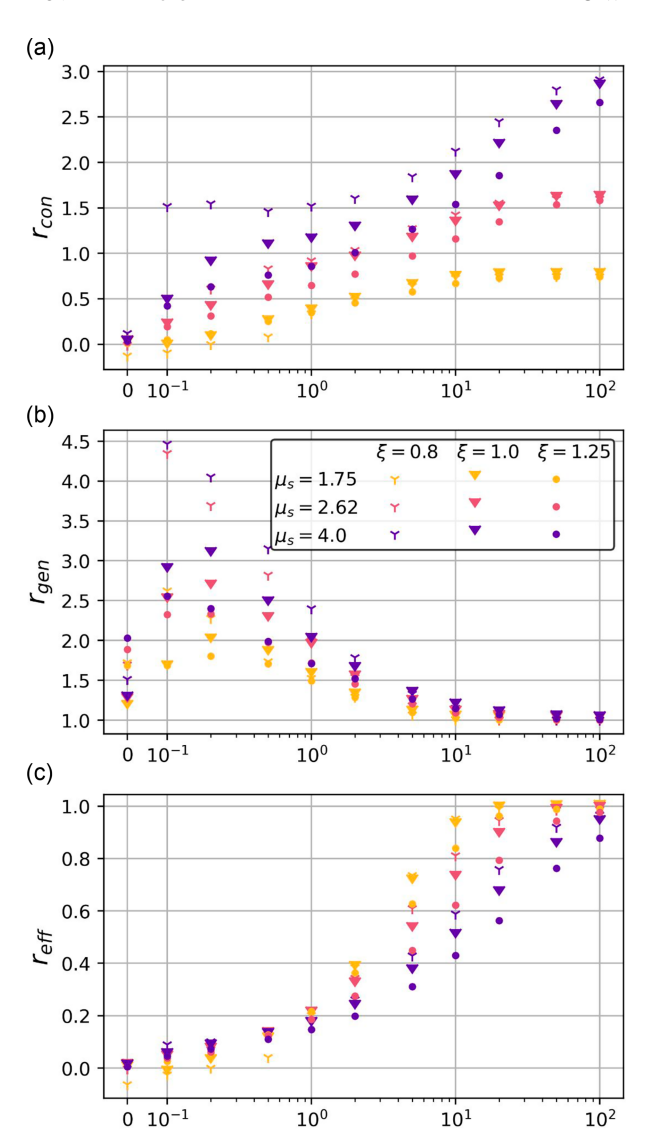


FIG. 6. (a) The conversion ratio  $r_{\rm con} = \langle \mathcal{P} \rangle / \langle \varepsilon_{\rm APE} \rangle$ , (b) the generation ratio  $r_{\rm gen} = D_m/D_d = \langle \varepsilon_{\rm APE} + \varepsilon_{\rm ME} \rangle / \mu_s \langle \varepsilon_{\rm APE} \rangle$ , (c) the moist conversion efficiency  $r_{\rm eff} = \langle \mathcal{P} \rangle / \langle \varepsilon_{\rm ME} \rangle = r_{\rm con} / (\mu_s r_{\rm gen} - 1)$ , all vs the evaporation constant E.

this is characterized by the turbulent diffusivity of the sensible heat across the inertial range of the inverse cascade, which directly predicts the total generation of EKE (e.g., Held and Larichev 1996). This concept can be extended for any quantity that acts as a passive tracer within an inertial range (Smith et al. 2002). In the MQG system, we define the dry diffusivity  $D_d$  and moist diffusivity  $D_m$  by

$$D_d = \frac{\langle v'_2 q'_{\rm bc} \rangle}{\overline{q_{\rm bc}}_y} = \frac{\langle \varepsilon_{\rm APE} \rangle}{U \lambda^{-2} g^* / 2H}, \tag{24}$$

$$D_{m} = \frac{\langle v_{2} q_{m}' \rangle}{\overline{q_{m_{v}}}} = \frac{\langle \varepsilon_{\text{APE}} + \varepsilon_{\text{ME}} \rangle}{\mu_{s} U \lambda^{-2} g^{*} / 2H}.$$
 (25)

Here, v' represents the meridional barotropic velocity anomaly, and  $q_{\rm bc}$  represents the baroclinic potential vorticity. The moist potential vorticity  $q_m$  is defined as in Brown et al. (2023) as

$$q_m = \zeta_{\rm bc} - \frac{f_0}{H} [\eta + (\mu_s - 1)\eta_c].$$
 (26)

We define a generation ratio as the ratio between the diffusivity for moist potential vorticity and that of the dry potential vorticity:

$$r_{\rm gen} = \frac{D_m}{D_d} = \frac{\langle \varepsilon_{\rm APE} + \varepsilon_{\rm ME} \rangle}{\mu_{\rm s} \langle \varepsilon_{\rm APE} \rangle}.$$
 (27)

Figure 6b plots the generation ratio as a function of evaporation rate. In the saturated limit, this ratio converges to 1, indicating that humidity and temperature have proportionate diffusivity at saturation. Equivalently, Brown et al. (2023) showed that at saturation,  $\langle \varepsilon_{\text{ME}} \rangle / \langle \varepsilon_{\text{APE}} \rangle = \mu_s - 1$ . At lower evaporation rates, the moist diffusivity is much higher than the dry diffusivity, increasing until near the dry limit. This portion increases as the dry criticality  $\xi$  decreases, and as the moisture gradient parameter  $\mu_s$  increases, peaking at either E = 0.1 or E = 0.2 in all configurations we tested. Systems with low evaporation (0.0 < E < 0.5), low baroclinicity ( $\xi$  = 0.8), and high moisture stratification ( $\mu_s \ge 2.62$ ) exhibit substantially higher generation ratios, indicating that latent heat accounts for a large portion of the heat transport in these systems. At higher evaporation rates, the configuration of the flow changes to a more wavelike pattern, qualitatively similar to classic baroclinic instability. Indeed, the high conversion ratio at low evaporation may result from isolated diabatic vortices that do not contribute much to the barotropic energy cascade and, consequently, do not drive an increase in the sensible heat flux. At very high evaporation, the system transitions to a more symmetric distribution of cyclones and anticyclones, which more easily generate an elongated cascade and large-scale sensible heat fluxes.

The low evaporation cases present an interesting contrast: Even though they are very efficient at moving moisture, as characterized by the generation ratio  $r_{\rm gen}$ , this enhanced moisture transport does not result in a large increase in the generation of kinetic energy, as measured by the low value of the conversion ration  $r_{\rm con}$ . We further quantify this discrepancy in terms of a moist conversion efficiency  $r_{\rm eff}$ , capturing the portion of EME converted into EAPE, as the ratio of the precipitation conversion to the total EME generation by the meridional flux:

$$r_{\rm eff} = \frac{\langle \mathcal{P} \rangle}{\langle \varepsilon_{\rm ME} \rangle} = \frac{r_{\rm con}}{\mu_s r_{\rm gen} - 1}.$$
 (28)

This loss ratio captures the transition from dry to moist geostrophic turbulence most dramatically, as it gradually increases from 0—meaning that most of the EME is never converted into EKE—to 1 in the saturated limit, where all the EME is converted into EKE. In a few cases with low evaporation and low moisture stratification, this term is negative, indicating that precipitation has a net negative effect on the APE. This feature distinguishes the moist conversion efficiency from traditional metrics of mechanical efficiency.

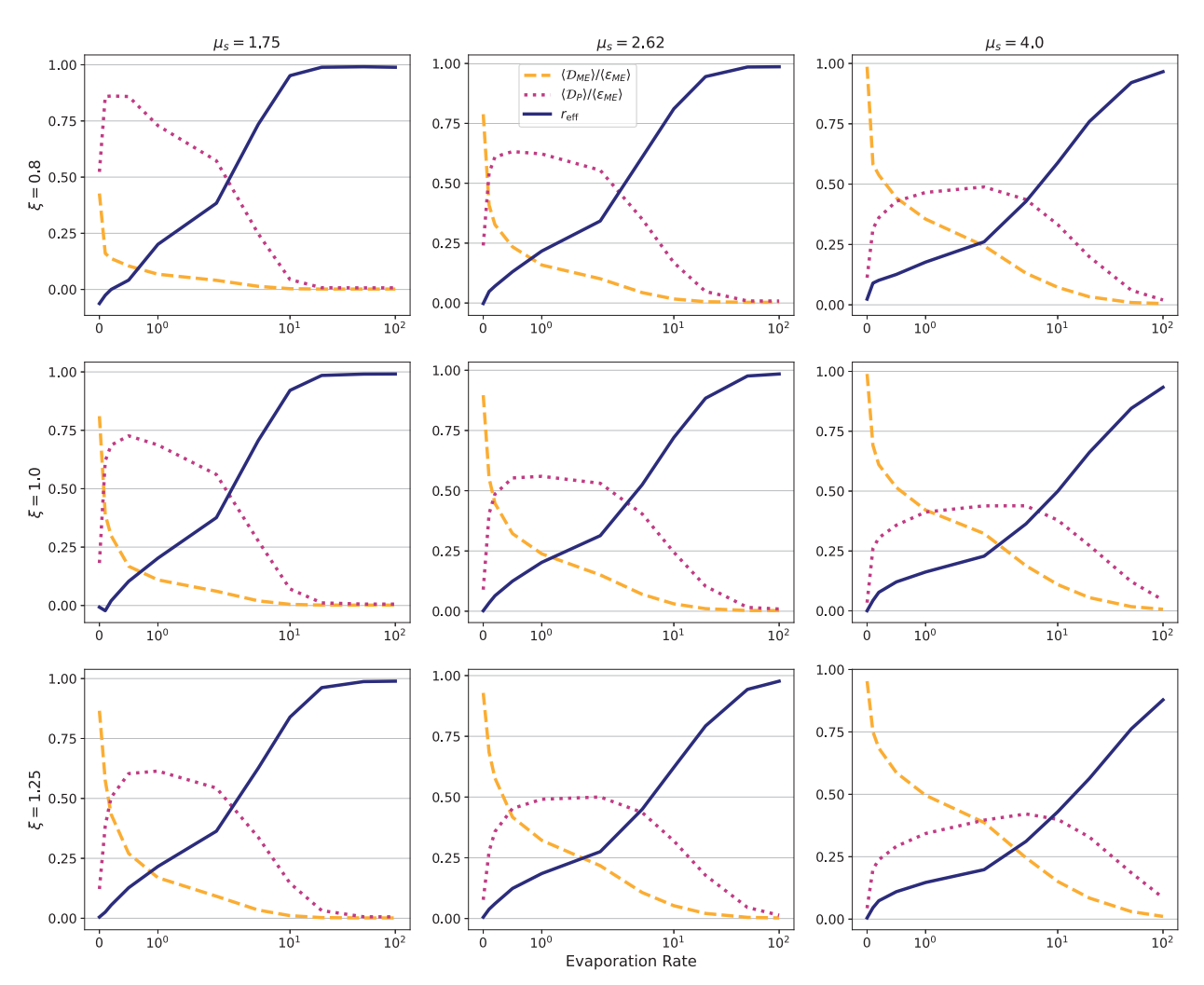


FIG. 7. The portion of generated EME lost to (i) small-scale diffusion (light dashed line), (ii) precipitation dissipation (pink dotted line), and (iii) the moisture conversion efficiency  $r_{\rm eff}$  (dark blue solid line), which captures conversion to APE via precipitation.

The results of Figs. 6b and 6c indicate that in partially saturated systems, only a fraction of the EME is converted into APE. Equation (15) indicates that the generation of EME by the meridional energy transport  $\varepsilon_{\text{ME}}$  is additionally removed through

- 1) Small-scale diffusion of moisture  $\mathcal{D}_{\rm ME},$  which dominates in dry turbulent systems
- 2) Eddy precipitation dissipation  $\mathcal{D}_p$ , which occurs in partially saturated systems

Figure 7 shows the time- and domain-averaged values of each sink term and the moisture conversion efficiency across the range of experiments. At the dry limit, moisture acts as a passive tracer in most of the domain, and hence the small-scale diffusion  $\mathcal{D}_{\text{ME}}$  dominates the removal of ME, except in subcritical systems that never fully equilibrate in our experiments (e.g.,  $\xi = 0.8$ ,  $\mu_s = 1.75$ ). For some simulations with low evaporation (e.g.,  $\xi = 0.8$ ,  $\mu_s = 1.75$  and E = 0.1), precipitation acts as a small source of ME, but a net sink of APE. Typically, precipitation acts as a sink of APE at larger scales,

arising from the tendency for the poleward transport of moisture to produce precipitation poleward of the jet and flatten the temperature gradient. Crucially, the small-scale diffusion  $\mathcal{D}_{\text{ME}}$  requires sufficiently strong turbulence for the cascade to mix anomalies in the condensation thickness to the diffusion scale.

The precipitation dissipation  $\mathcal{D}_p$  is a significant sink of EME at intermediate evaporation rates. This is most significant in the simulations that are subcritical in the dry scenario, where  $\mathcal{D}_p$  accounts for ~90% of the loss in the  $\xi = 0.8$ ,  $\mu_s = 1.75$ , E = 0.1, 0.2 simulations. For evaporation rate sweeps at higher dry criticality with  $\mu_s = 1.75$ , precipitation dissipation is strongest at higher evaporation rates (E = 0.5 and E = 0.1 for  $\xi = 1.0$ , 1.25, respectively) and accounts for a smaller portion of the EME loss (~70% and 60% for  $\xi = 1.0$ , 1.25, respectively). A similar shift occurs when increasing moisture stratification. In the simulation with the steepest moisture and temperature gradients ( $\xi = 1.25$ ,  $\mu_s = 4.0$ ), the peak occurs at E = 5.0 and accounts for only 40% of the energy loss. Small-scale diffusion compensates for the reduction and, consequently,

the moisture conversion efficiency is also smaller than simulations with the same evaporation but shallower temperature and moisture gradients.

Eddy precipitation dissipation also explains why low baroclinicity ( $\xi = 0.8$ ), low evaporation (0.0 < E < 0.5) simulations have significantly different conversion ratios despite similar generation ratios. In particular, precipitation dissipation accounts for more than half of the loss of EME when  $\mu_s \le 2.62$ . For the  $\mu_s = 4.0$  simulations, precipitation dissipation is smaller, and moisture conversion efficiency is larger, with small-scale diffusion as the dominant source of inefficiency. As the midlatitude atmosphere corresponds to a MQG system with moist stability of about 1.7-2.6, precipitation dissipation may play a significant role in regulating the scale distribution of moisture on Earth. With higher moisture stratification, small meridional displacements of moist air generate highly localized latent heat release within a domain that is largely subsaturated. This mixes moisture to smaller scales, further favoring localized latent heat release. In systems with lower moisture stratification, moisture must be transported further before latent heat is released. In systems with steeper temperature gradients, baroclinic instability increases the downgradient flux of sensible heat, decreasing both the conversion and generation ratios.

#### 6. Discussion

We now attempt to more broadly characterize the energetics as a function of all key parameters. Figure 8 plots isolines of each loss mechanism as a function of evaporation and effective saturated criticality. Small-scale diffusion tends to dominate at high saturated criticality and low evaporation. Precipitation dissipation dominates at lower saturated criticality and intermediate evaporation. Isolines of small-scale diffusion are steepest at low evaporation and become more shallow as evaporation increases. Isolines of precipitation dissipation are steepest at low evaporation and between E = 2 and E = 5, with a region of intermediate evaporation where the slope of isolines is near zero. For larger values of E, isolines of moisture dissipation have a shallower slope with increasing E. Moisture conversion efficiency  $r_{\rm eff}$  is negative for low evaporation and small saturated criticality (bottom-left corner): latent heat release is a net sink of APE in this region of parameter space.

We define three limiting regimes based on the moisture conversion efficiency and the dominant mechanism generating inefficiency:

- 1) Regime 1, a dry regime corresponding to low evaporation rates and higher saturated criticality. Here, small-scale diffusion  $\mathcal{D}_{\text{ME}}$  dominates the loss of ME, and the system has low moist conversion efficiency. In Fig. 8, this occurs in the yellow-hatched regions.
- 2) Regime 2, corresponding to intermediate evaporation rates and lower saturated criticality. Here,  $\mathcal{D}_P$  dominates the loss of ME, and the system has intermediate moist conversion efficiency. In Fig. 8, this occurs in the dotted pink region.
- Regime 3, a "saturated" regime corresponding to high evaporation. Here, almost all generated EME is converted

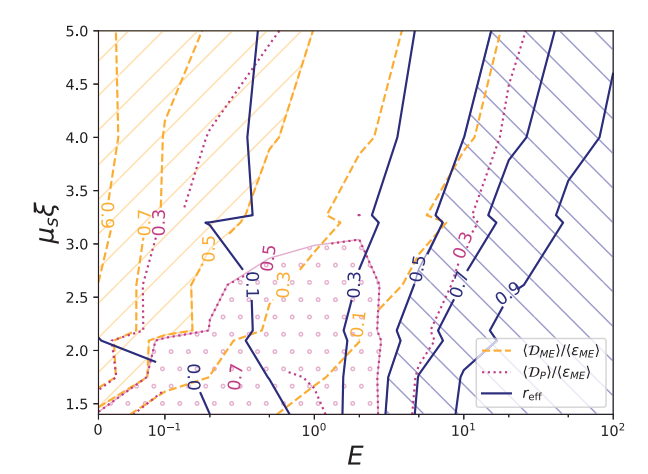


FIG. 8. Approximate isolines of the relative contribution of each EME sink as a function of the saturated criticality  $\mu_s \xi$  and the evaporation rate E. In the hatched regions, a single process accounts for more than half of the EME loss. Small-scale diffusion (yellow) dominates at low evaporation and high saturated criticality. Precipitation dissipation (pink) dominates at intermediate evaporation and low saturated criticality. Moisture conversion efficiency (blue) approaches 1 at very high evaporation, with more evaporation required for higher saturated criticality.

into EAPE through precipitation  $\mathcal{P}$ . The system is therefore highly efficient at converting moisture into EKE. In Fig. 8, the system approaches this limit in the blue-hatched region.

The three limiting regimes do not cover all of parameter space. In the middle of Fig. 8, regions without hatching, the flow exhibits features of all three regimes and cannot be characterized by a single dominant process.

To gain insight into the dynamical implications of each regime, we modify turbulence theory to take into account the nonlinearity of precipitation. If moisture behaves purely as a passive tracer (as is nearly achieved in regime 1), the turbulent flow mixes moisture downgradient, generating variance in the moisture deficit. A more turbulent flow, corresponding to a higher value of  $\xi$ , generates larger variance due to the stronger forward cascade. This accounts for the diagonal tilt of the lines delineating different regimes. Because the "dry like" regime allows the forward cascade of moisture to continue to the diffusion scale without precipitation disrupting the cascade near the Rossby scale (not shown), there is a large variance in the moisture distribution down to very small scales. This regime thus favors small-scale precipitation anomalies that lead to vortices like those found in the left column of Fig. 3.

In regime 2, precipitation dissipation becomes the dominant sink of EME. The condensation process selectively removes moisture surpluses, introducing skewness to the distribution and decreasing the mean and variance moisture deficit. This regime contains many instances of precipitation having a negative contribution to the EAPE and a positive contribution to the EME. A large precipitation dissipation term more than counteracts the positive forcing of precipitation in the EME, and thus precipitation in this regime results in a loss of EAPE without a corresponding gain in EME. In regime 3, the system

begins to behave more similarly to the saturated limit discussed in Brown et al. (2023), dominated by precipitation-driven exchanges between the EME and EAPE.

### a. Turbulent mixing and relative humidity

The energetic output of MQG is governed by the competition between the generation of moisture variance by turbulent processes and its removal by moist processes. The reduced impact of moisture diffusion in more saturated systems suggests that precipitation halts the forward cascade when sufficient moisture is available. We use this observation in conjunction with turbulence theory to demonstrate how the moisture conversion efficiency relates to the relative humidity.

Let us assume that the moisture deficit is Gaussian in its distribution, with mean value

$$d_0 = \langle \eta_{c,0} - \eta_0 \rangle, \tag{29}$$

and variance

$$\sigma_d = \langle (\eta_c' - \eta')^2 \rangle^{1/2}, \tag{30}$$

defined by the root-mean-square (RMS) deficit perturbation. Condensation occurs in the regions, where  $\eta_c - \eta > 0$ . We quantify this portion of the domain by  $\alpha \approx \int_0^\infty \phi(x,d_0,\sigma_d)dx$ , where  $\phi(x,d_0,\sigma_d)$  is the normal distribution of the deficit  $x=\eta_c-\eta$  with mean value  $d_0$  and standard deviation  $\sigma_d$ . Intuitively, the value of this integral depends on the parameter  $d_0/\sigma_d$ . When a smaller fraction of the domain is saturated,  $d_0/\sigma_d$  is more negative, and the average relative humidity is lower.

The dominant mechanisms of EME loss are strongly correlated with  $d_0/\sigma_d$ , as shown in Fig. 9. This diagnostic parameter allows us to collapse the integrations onto single curves, although less perfectly for lower values of  $\mu_s$ . For low values below -1.5, the mean relative humidity approaches 0, and the system is effectively dry with precipitation as a rare event (regime 1). Regime 2, dominated by precipitation dissipation, appears for values between -1 and -0.5. Here, the mean relative humidity is roughly one standard deviation from saturation, so precipitation is common, but most of the domain remains subsaturated. As  $d_0/\sigma_d$  approaches 0, the system transitions to the saturated regime 3 with relative humidity near 1 everywhere.

While the relative importance of precipitation dissipation and small-scale diffusion largely converge for similar values of the distribution parameter  $d_0/\sigma_d$ , the precipitation dissipation exhibits a wide range. Smaller moisture  $\mu_s$  and temperature gradients  $\xi$  are correlated with larger precipitation dissipation. Indeed, the systems with the largest moisture stratification ( $\mu_s = 4.0$ ) never lose a majority of the EME to precipitation dissipation and instead occupy a regime where all three sinks are of comparable size. In contrast, the simulations with the smallest moisture stratification ( $\mu_s = 1.75$ ) lose over 80% of their EME to precipitation dissipation. When the evaporation rate is also low, precipitation can have a net negative effect on the EAPE (the bottom-left corner of Fig. 8).

The dynamics of the MQG system are determined by the size of the mean moisture deficit relative to the RMS deficit variance. The moisture deficit of the MQG system can be related to the relative humidity of the atmosphere. Thus, relative

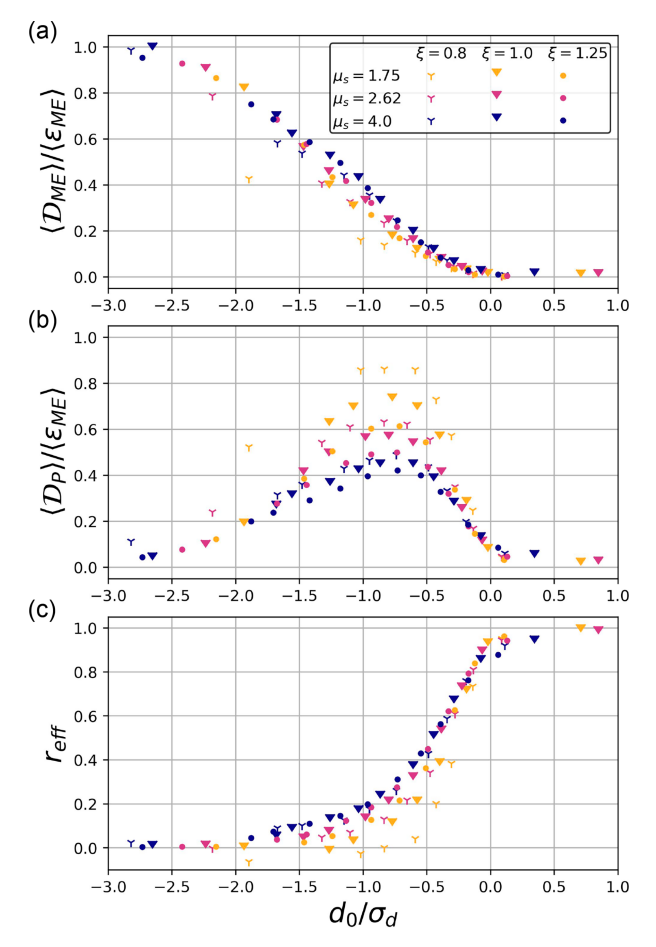


FIG. 9. The fractional loss of EME due to (a) small-scale diffusion, (b) domain-scale diffusion, and (c) precipitation conversion as a function of the ratio between the mean deficit and the RMS deficit variance. (c) Equivalent to the moisture conversion efficiency.

humidity plays a critical role in setting the moisture conversion efficiency (Fig. 9c): A drier atmosphere is less able to convert moisture gradients into eddy kinetic energy.

# b. Climate estimates for the evaporation constant

Where do our current and potential future climates fall within the parameter space of Fig. 8? Lapeyre and Held (2004) estimate that realistic parameter values are near E = 0.4 and  $\mu_s \xi \in (1.75, 2.62)$ , the bounds corresponding to average winter and summer limits, respectively. Estimating changes under warming is difficult due to feedbacks between moist and dry processes. Nonetheless, we can synthesize the results of a few studies for a qualitative prediction of changes to the evaporation parameter.

The evaporation constant E is defined as

$$E = \frac{f_0 \lambda^2}{U^2 m_0} E^*$$

$$= \frac{E^*}{m_0} \times \frac{\lambda^2 \beta}{U} \times \frac{f_0}{\beta U}$$

$$= \frac{1}{\tau_E} \times \frac{1}{\xi} \times \tau_{\xi}.$$
(31)

In the third line, we have decomposed this constant into three terms:

- 1) The first term is the inverse of an evaporation time scale  $\tau_E = E^*/m_0$ . Following Held and Soden (2006), the evaporation rate  $E^*$  increases more slowly than Clausius–Clapeyron, while the typical moisture content  $m_0$  scales with the Clausius–Clapeyron relationship. In a warmer climate, we therefore expect this term to decrease.
- 2) The second term is the inverse of the criticality for dry baroclinic instability. Stone (1978) argues that the extratropical atmosphere adjusts to marginal criticality  $\xi \approx 1$ . If this remains the case in a warmer world, we would expect the supercriticality to remain unchanged. However, we note that this assumption neglects the impact of moist processes, which may generate moist baroclinic adjustment under dry configurations that would otherwise be stable. In this case, the criticality may decrease, slightly increasing E.
- 3) The last term is a vorticity advection time scale. Changes to this time scale are governed by changes to the wind shear *U*. Shaw and Miyawaki (2024) argue that the impact of moisture leads to an increase in the thermal wind, which predominantly impacts the fastest winds of the jet stream. If this reflects global changes to the mean wind shear, this time scale should decrease.

We thus expect that in a warmer planet, the nondimensional evaporation parameter decreases. Counterintuitively, this indicates that the midlatitude dynamics will shift toward a more dry-like regime, and precipitation will have a less positive, or possibly even negative impact on the EKE. Crucially, though we expect the actual evaporation to increase modestly in a warmer world, the increase is limited by the energy balance at the surface and cannot keep up with the increase in total moisture, which scales with the Clausius–Clapeyron relation. The primary drivers for this shift are the slowing down of the hydrological cycles (Held and Soden 2006) and the intensification of the thermal wind (Shaw and Miyawaki 2024). A more detailed study is necessary to rigorously quantify the effect.

### 7. Conclusions

We demonstrated that the relative humidity of the atmosphere, as determined by the surface evaporation rate, greatly impacts the intensity of midlatitude eddies. Building upon the energetic framework of Brown et al. (2023) for the MQG equations, we analyzed the sensitivity of the generation of kinetic energy by geostrophic turbulence to the evaporation rate. We found that as evaporation increases, moist geostrophic turbulence gradually transitions from a dry limit  $(E \rightarrow 0)$  characterized by low level of kinetic energy to a saturated limit  $(E \to \infty)$ with much more intense turbulence. At low evaporation rates, systems with lower moisture stratification exhibit a reduction in total energetic output compared with the dry limit, a result previously only shown in nonhomogeneous moist systems (e.g., Bembenek et al. 2020; Lutsko and Hell 2021). Systems with higher moisture stratification remain at roughly the same energetic output. Further increases in evaporation lead to a rapid increase in EKE in all systems, with higher baroclinicity and

gross moisture stratification corresponding to a more rapid increase (Fig. 4). As each system approaches a saturated limit, the energetic output levels off. Systems with higher baroclinicity and gross moisture stratification require more evaporation to reach this limit.

The generation of kinetic energy by moist geostrophic turbulence is tied to the meridional transport of latent and sensible heat. By transporting moisture poleward, eddies extract ME from the background gradient and convert it into APE through precipitation. This conversion is inefficient in that only a fraction of ME is converted to kinetic energy. It becomes increasingly efficient as evaporation increases relative humidity, with all EME being converted into EKE in the saturated limit. Stronger turbulent dynamics reduce the efficiency of conversion, resulting in a tug of war on the total efficiency between competing processes of moisture availability and turbulent mixing. We defined a "moist conversion efficiency" by expanding upon existing metrics characterizing the relative contribution of dry and moist processes: the conversion ratio of Parker and Thorpe (1995) and a generation ratio defined by the relative strength of the moist static energy flux to the dry static energy flux.

The inefficient conversion of ME to kinetic energy arises from the fact that EME is dissipated through small-scale diffusion and eddy-scale precipitation diffusion. The former dominates when the system is sufficiently turbulent (driving the elongation of the forward cascade of ME) and sufficiently dry (lest precipitation halt the cascade before the dissipation scale). The latter dominates when the system is roughly balanced between regions of saturation and deficit, such that ME is lost through the selective flattening of surplus anomalies by precipitation.

We showed that the dominant mechanism of ME loss is correlated with the ratio of the mean moisture deficit to the moisture deficit variability  $d_0/\sigma_d$  capturing the availability of moisture relative to the strength of turbulent mixing. When the mean deficit is large compared to the variance (with a ratio less than  $\sim -1.5$ ), precipitation is sparse and highly localized, leading to a system with mostly dry behavior but some localized storms. For ratios between -1 and -0.5, precipitation becomes more widespread, leading to a regime dominated by precipitation dissipation. As this ratio approaches 0, the crossover from a mean deficit to a surplus, the system approaches the saturated limit, and most of the ME is converted into APE.

Our results indicate that diabatic processes play a large role in setting the scale distribution of energy in the atmosphere. Indeed, MQG may underestimate the size of that role. Notably, precipitation dissipation  $\mathcal{D}_P \propto \tau P^2$  vanishes in the limit  $\tau \to 0$ . A longer precipitation relaxation time scale would further decrease efficiency. Evaporation similarly dissipates EME. This term disappears with uniform evaporation (as considered in our idealized model), but more realistic evaporation based on the surface flux would yield an additional dissipation term of the form:

$$\mathcal{D}_F \propto |U_2| d^2. \tag{32}$$

The effect of these additional dissipation terms is likely to lead to greater reduction of the moisture variance than found here, further correlating moisture and temperature.

While the MQG system is highly idealized, the impacts of relative humidity on the generation of kinetic energy in geostrophic turbulence have also been noted in moist convection (Pauluis and Held 2002a; Pauluis 2011; Singh and O'Gorman 2016), tropical cyclones (Pauluis and Zhang 2017), and the global circulation (Laliberté et al. 2015). Furthermore, the mathematical expressions for dissipation by diffusion and precipitation in MQG correspond with the irreversible entropy production entropy due to diffusion of water vapor and irreversible phase changes. These strongly indicate that our findings are not an artifact of the MQG system but reflect the physical sensitivity of moist eddies to the relative humidity of the atmosphere. Homogeneous models remain relevant for studying the energetic output relative to a saturated state, even if they exhibit different trends than nonhomogeneous models (Lutsko et al. 2024).

Furthermore, we have defined metrics that can be calculated explicitly for a range of models and observations. The conversion and generation ratios are computed from quantities discussed in previous studies of moist dynamics (e.g., Chang et al. 2002; Fig. 8) combined with the gross moist stability of Neelin and Held (1987). The moist conversion efficiency is computed from a combination of these quantities. Similarly, the ratio between the mean moisture deficit and its variability can be calculated from the difference between the humidity and its saturation value, which can be computed globally or regionally (e.g., just in the storm tracks). Future work can thus verify and connect the results of our study with more complex models and the atmosphere.

Acknowledgments. This research was supported in part by the U.S. NSF through Award OAC-2004572 and the NYU IT High-Performance Computing resources, services, and staff expertise. We thank Pablo Zurita-Gotor and two anonymous reviewers for helpful comments.

Data availability statement. The code used to generate the data in this study is stored in the repository at https://github.com/margueriti/Moist OG public.

### REFERENCES

- Adames, Á. F., and Y. Ming, 2018: Interactions between water vapor and potential vorticity in synoptic-scale monsoonal disturbances: Moisture vortex instability. J. Atmos. Sci., 75, 2083–2106, https://doi.org/10.1175/JAS-D-17-0310.1.
- Barry, L., G. C. Craig, and J. Thuburn, 2002: Poleward heat transport by the atmospheric heat engine. *Nature*, 415, 774–777, https://doi.org/10.1038/415774a.
- Bembenek, E., D. N. Straub, and T. M. Merlis, 2020: Effects of moisture in a two-layer model of the midlatitude jet stream. *J. Atmos. Sci.*, 77, 131–147, https://doi.org/10.1175/JAS-D-19-0021.1.
- Brown, M. L., O. Pauluis, and E. P. Gerber, 2023: Scaling for saturated moist quasigeostrophic turbulence. *J. Atmos. Sci.*, **80**, 1481–1498, https://doi.org/10.1175/JAS-D-22-0215.1.
- Chang, E. K. M., S. Lee, and K. L. Swanson, 2002: Storm track dynamics. J. Climate, 15, 2163–2183, https://doi.org/10.1175/ 1520-0442(2002)015<02163:STD>2.0.CO;2.

- Chemke, R., Y. Ming, and J. Yuval, 2022: The intensification of winter mid-latitude storm tracks in the Southern Hemisphere. *Nat. Climate Change*, 12, 553–557, https://doi.org/10.1038/s41558-022-01368-8.
- Emanuel, K. A., 1985: Frontal circulations in the presence of small moist symmetric stability. J. Atmos. Sci., 42, 1062–1071, https:// doi.org/10.1175/1520-0469(1985)042<1062:FCITPO>2.0.CO;2.
- —, M. Fantini, and A. J. Thorpe, 1987: Baroclinic instability in an environment of small stability to slantwise moist convection. Part I: Two-dimensional models. *J. Atmos. Sci.*, 44, 1559–1573, https://doi.org/10.1175/1520-0469(1987)044<1559: BIIAEO>2.0.CO:2.
- Frierson, D. M. W., 2006: Robust increases in midlatitude static stability in simulations of global warming. *Geophys. Res. Lett.*, **33**, L24816, https://doi.org/10.1029/2006GL027504.
- —, I. M. Held, and P. Zurita-Gotor, 2006: A gray-radiation aquaplanet moist GCM. Part I: Static stability and eddy scale. J. Atmos. Sci., 63, 2548–2566, https://doi.org/10.1175/JAS3753.1.
- Held, I. M., and V. D. Larichev, 1996: A scaling theory for horizontally homogeneous, baroclinically unstable flow on a beta plane. J. Atmos. Sci., 53, 946–952, https://doi.org/10.1175/1520-0469(1996)053<0946:ASTFHH>2.0.CO;2.
- —, and B. J. Soden, 2006: Robust responses of the hydrological cycle to global warming. *J. Climate*, **19**, 5686–5699, https://doi. org/10.1175/JCLI3990.1.
- Juckes, M. N., 2000: The static stability of the midlatitude troposphere: The relevance of moisture. J. Atmos. Sci., 57, 3050–3057, https://doi.org/10.1175/1520-0469(2000)057<3050:TSSOTM>2. 0.CO:2.
- Kang, J. M., T. A. Shaw, S. M. Kang, I. R. Simpson, and Y. Yu, 2024: Revisiting the reanalysis-model discrepancy in Southern Hemisphere winter storm track trends. *npj Climate Atmos*. *Sci.*, 7, 252, https://doi.org/10.1038/s41612-024-00801-3.
- Kohl, M., and P. A. O'Gorman, 2022: The diabatic Rossby vortex: Growth rate, length scale, and the wave–vortex transition. J. Atmos. Sci., 79, 2739–2755, https://doi.org/10.1175/JAS-D-22-0022.1.
- Laliberté, F., J. Zika, L. Mudryk, P. J. Kushner, J. Kjellsson, and K. Döös, 2015: Constrained work output of the moist atmospheric heat engine in a warming climate. *Science*, 347, 540– 543, https://doi.org/10.1126/science.1257103.
- Lambaerts, J., G. Lapeyre, and V. Zeitlin, 2011: Moist versus dry barotropic instability in a shallow-water model of the atmosphere with moist convection. *J. Atmos. Sci.*, 68, 1234–1252, https://doi.org/10.1175/2011JAS3540.1.
- Lapeyre, G., and I. M. Held, 2004: The role of moisture in the dynamics and energetics of turbulent baroclinic eddies. *J. Atmos. Sci.*, **61**, 1693–1710, https://doi.org/10.1175/1520-0469(2004)061<1693:TROMIT>2.0.CO;2.
- Lorenz, D. J., and E. T. DeWeaver, 2007: Tropopause height and zonal wind response to global warming in the IPCC scenario integrations. *J. Geophys. Res.*, 112, D10119, https://doi.org/10. 1029/2006JD008087.
- Lorenz, E. N., 1978: Available energy and the maintenance of a moist circulation. *Tellus*, 30 (1), 15–31, https://doi.org/10.1111/ j.2153-3490.1978.tb00815.x.
- Lutsko, N. J., and M. C. Hell, 2021: Moisture and the persistence of annular modes. *J. Atmos. Sci.*, **78**, 3951–3964, https://doi.org/10.1175/JAS-D-21-0055.1.
- —, J. Martinez-Claros, and D. D. B. Koll, 2024: Atmospheric moisture decreases midlatitude eddy kinetic energy. *J. Atmos. Sci.*, 81, 1817–1832, https://doi.org/10.1175/JAS-D-23-0226.1.

- Merlis, T. M., and Coauthors, 2024: Climate sensitivity and relative humidity changes in global storm-resolving model simulations of climate change. *Sci. Adv.*, **10**, eadn5217, https://doi.org/10.1126/sciadv.adn5217.
- Moore, R. W., and M. T. Montgomery, 2004: Reexamining the dynamics of short-scale, diabatic Rossby waves and their role in midlatitude moist cyclogenesis. *J. Atmos. Sci.*, **61**, 754–768, https://doi.org/10.1175/1520-0469(2004)061<0754:RTDOSD>2. 0.CO;2.
- —, and —, 2005: Analysis of an idealized, three-dimensional diabatic Rossby vortex: A coherent structure of the moist baroclinic atmosphere. J. Atmos. Sci., 62, 2703–2725, https:// doi.org/10.1175/JAS3472.1.
- ——, and H. C. Davies, 2008: The integral role of a diabatic Rossby vortex in a heavy snowfall event. *Mon. Wea. Rev.*, **136**, 1878–1897, https://doi.org/10.1175/2007MWR2257.1.
- Neelin, J. D., and I. M. Held, 1987: Modeling tropical convergence based on the moist static energy budget. *Mon. Wea. Rev.*, **115**, 3–12, https://doi.org/10.1175/1520-0493(1987)115<0003: MTCBOT>2.0.CO;2.
- O'Gorman, P. A., 2010: Understanding the varied response of the extratropical storm tracks to climate change. *Proc. Natl. Acad. Sci. USA*, **107**, 19176–19180, https://doi.org/10.1073/pnas.1011547107.
- —, and T. Schneider, 2008: Energy of midlatitude transient eddies in idealized simulations of changed climates. *J. Climate*, 21, 5797–5806, https://doi.org/10.1175/2008JCLI2099.1.
- —, T. M. Merlis, and M. S. Singh, 2018: Increase in the skewness of extratropical vertical velocities with climate warming: Fully nonlinear simulations versus moist baroclinic instability. *Quart. J. Roy. Meteor. Soc.*, **144**, 208–217, https://doi.org/10.1002/qj.3195.
- Parker, D. J., and A. J. Thorpe, 1995: Conditional convective heating in a baroclinic atmosphere: A model of convective frontogenesis. *J. Atmos. Sci.*, 52, 1699–1711, https://doi.org/10. 1175/1520-0469(1995)052<1699:CCHIAB>2.0.CO;2.
- Pauluis, O., 2011: Water vapor and mechanical work: A comparison of Carnot and steam cycles. J. Atmos. Sci., 68, 91–102, https://doi.org/10.1175/2010JAS3530.1.
- —, and I. M. Held, 2002a: Entropy budget of an atmosphere in radiative–convective equilibrium. Part I: Maximum work and frictional dissipation. *J. Atmos. Sci.*, **59**, 125–139, https://doi. org/10.1175/1520-0469(2002)059<0125:EBOAAI>2.0.CO;2.
- —, and —, 2002b: Entropy budget of an atmosphere in radiative-convective equilibrium. Part II: Latent heat transport and moist processes. *J. Atmos. Sci.*, **59**, 140–149, https://doi.org/ 10.1175/1520-0469(2002)059<0140:EBOAAI>2.0.CO;2.

- Pauluis, O. M., and F. Zhang, 2017: Reconstruction of thermodynamic cycles in a high-resolution simulation of a hurricane. J. Atmos. Sci., 74, 3367–3381, https://doi.org/10.1175/JAS-D-16-03531.
- Pavan, V., N. Hall, P. Valdes, and M. Blackburn, 1999: The importance of moisture distribution for the growth and energetics of mid-latitude systems. *Ann. Geophys.*, 17, 242–256, https://doi.org/10.1007/s00585-999-0242-y.
- Schneider, T., and P. A. O'Gorman, 2008: Moist convection and the thermal stratification of the extratropical troposphere. *J. Atmos.* Sci., 65, 3571–3583, https://doi.org/10.1175/2008JAS2652.1.
- Shaw, T. A., and O. Miyawaki, 2024: Fast upper-level jet stream winds get faster under climate change. *Nat. Climate Change*, 14, 61–67, https://doi.org/10.1038/s41558-023-01884-1.
- —, and Coauthors, 2016: Storm track processes and the opposing influences of climate change. *Nat. Geosci.*, 9, 656–664, https://doi.org/10.1038/ngeo2783.
- Sherwood, S. C., W. Ingram, Y. Tsushima, M. Satoh, M. Roberts, P. L. Vidale, and P. A. O'Gorman, 2010: Relative humidity changes in a warmer climate. *J. Geophys. Res.*, 115, D09104, https://doi.org/10.1029/2009JD012585.
- Singh, M. S., and P. A. O'Gorman, 2016: Scaling of the entropy budget with surface temperature in radiative-convective equilibrium. J. Adv. Model. Earth Syst., 8, 1132–1150, https://doi. org/10.1002/2016MS000673.
- Smith, K. S., G. Boccaletti, C. C. Henning, I. Marinov, C. Y. Tam, I. M. Held, and G. K. Vallis, 2002: Turbulent diffusion in the geostrophic inverse cascade. *J. Fluid Mech.*, 469, 13–48, https://doi.org/10.1017/S0022112002001763.
- Soden, B. J., and I. M. Held, 2006: An assessment of climate feed-backs in coupled ocean–atmosphere models. *J. Climate*, 19, 3354–3360, https://doi.org/10.1175/JCLI3799.1.
- Stone, P. H., 1978: Baroclinic adjustment. *J. Atmos. Sci.*, **35**, 561–571, https://doi.org/10.1175/1520-0469(1978)035<0561:BA>2.
- Wernli, H., S. Dirren, M. A. Liniger, and M. Zillig, 2002: Dynamical aspects of the life cycle of the winter storm 'Lothar' (24–26 December 1999). Quart. J. Roy. Meteor. Soc., 128, 405–429, https://doi.org/10.1256/003590002321042036.
- Whitaker, J. S., and C. A. Davis, 1994: Cyclogenesis in a saturated environment. *J. Atmos. Sci.*, **51**, 889–908, https://doi.org/10.1175/1520-0469(1994)051<0889:CIASE>2.0.CO;2.
- Zurita-Gotor, P., 2005: Updraft/downdraft constraints for moist baroclinic modes and their implications for the short-wave cutoff and maximum growth rate. J. Atmos. Sci., 62, 4450– 4458, https://doi.org/10.1175/JAS3630.1.